Plasma Physics and Controlled Fusion

PAPER

Influence of plasma background on 3D scrape-off layer filaments

To cite this article: D Schwörer *et al* 2019 *Plasma Phys. Control. Fusion* **61** 025008

IOP Publishing Plasma Physics and Controlled Fusion
Plasma Phys. Control. Fusion **61** (2019) 025008 (12pp) https://doi.org/10.1088/1361-6587/aae8fe

Influence of plasma background on 3D scrape-off layer filaments

D Schwörer[1,2], N R Walkden[2], H Leggate[1], B D Dudson[3], F Militello[2], T Downes[1] and M M Turner[1]

[1] Dublin City University, Dublin 9, Ireland
[2] CCFE, Culham Science Centre, Abingdon, Oxfordshire, OX14 3DB, United Kingdom
[3] York University, York, Yorkshire, YO10 5DD, United Kingdom

E-mail: david.schworer2@mail.dcu.ie

Received 15 June 2018, revised 3 October 2018
Accepted for publication 17 October 2018
Published 6 December 2018

Abstract

This paper presents the effect of self-consistent plasma backgrounds, including plasma–neutral interactions, on the dynamics of filament propagation. The principle focus is on the influence of the neutrals on the filament through both direct interactions and through their influence on the plasma background. Both direct and indirect interactions influence the motion of filaments. A monotonic increase of filament peak velocity with upstream electron temperature is observed, while a decrease with increasing electron density is observed. If ordered by the target temperature, the density dependence disappears and the filament velocity is only a function of the target temperature. Smaller filaments maintain a density dependence as a result of the density dependence of the plasma viscosity. The critical size δ^*, where filaments are at their fastest, is shifted to larger sizes for higher densities due to the plasma viscosity. If the density dependence of the plasma viscosity is removed, δ^* has no density dependence, but rather a temperature dependence.

Keywords: scrape-off layer, transport, neutrals, filaments, self-consistent, plasma

(Some figures may appear in colour only in the online journal)

1. Introduction

Filaments are field-aligned non-linear pressure perturbations that have been observed in most magnetized plasmas [1]. These intermittent, localized objects have a much smaller cross-section perpendicular to the magnetic field than parallel. In tokamaks, they can carry a significant amount of heat and particles to the first wall materials, which may cause sputtering, thereby diluting the plasma and degrading the wall. The plasma–wall interaction can cause dust production as well as increase tritium retention—both concerns for ITER [2]. Further filaments contribute to the cross field transport in the scrape-off layer (SOL), which influences the width of the SOL and affects the power handling at the divertor [3, 4]. Understanding filaments with a view to predicting and controlling them in future devices is therefore of interest.

The computer simulation of filaments was conducted initially in 2D [5–7]. In the 2D simulations, closures are needed due to the lack of resolution in the parallel direction. The two commonly used closures are sheath dissipation closure, neglecting parallel gradients, or the vorticity advection closure, neglecting parallel currents. Both cannot reproduce the results from full 3D simulation [8–10]. Boltzmann spinning and the associated poloidal motion is also not observed with 2D closures [8]. Further, drift waves cannot be captured properly by 2D simulation [11]. Moving towards a more complete picture of the physics, the complexity of simulations was further increased. For example, finite thermal perturbation can significantly influence filament dynamics, as it increases the poloidal motion and decreases the radial velocity [12, 13]. For a more complete review of both the computational advances, as well as experimental observations, see the review given in [1].

Neutral–plasma interactions are important for the operation of fusion devices, in particular for detached operation, where neutrals dissipate the majority of the parallel heat fluxes in the divertor region. Also, in the attached regime, neutrals can have a significant influence on plasma dynamics.

Compared to present day machines, future fusion devices will have an increased density in the divertor. This further increases the importance of understanding the influence of neutral plasma interactions in the divertor. Plasma–wall interaction is a key issue, not only for the operation of ITER, but also for future fusion devices. Therefore increasing the understanding of filaments, one of the main transport mechanisms in the SOL, is needed, especially in the presence of neutrals. Plasma turbulence interactions with neutral studies have recently been conducted [14–16]. Leddy *et al* [14] have shown that the neutral interaction can be increased by resolving the fluctuations compared to the mean field approach. Bisai and Kaw [15] show that neutrals can reduce electric fields, reduce fluctuations and increase pressure gradients in the SOL. In terms of filament–neutral interaction, a recent study showed that filaments can significantly increase the fuelling of the core by creating energetic neutrals [17]. Scaling laws, describing the filament radial velocity as a function of the plasma background parameter, have been derived [6, 7, 12]. Theiler *et al* derived a scaling including neutral plasma friction [18]. The scalings, however, simplify the equations in various ways to obtain an analytic expression for the filament velocity.

The study presented here extends this by taking not only the plasma–neutral interaction into account, but further looking at self consistent parallel background profiles which include parallel gradients. By looking at both direct and indirect interactions between filaments and the neutral population, these simulations extend the earlier study of direct interactions [19]. By looking at the influence of background profiles, earlier studies examining the influence of resistivity are extended in a self consistent way [20].

The equations and the setup used here are described in section 2, followed by a short introduction to the background profiles in section 3. The 3D dynamics of the simulated filaments is discussed in section 4. This is followed by the influence of the neutrals, the background profiles in general, and the filament size in section 5, before the summary in section 6.

2. Modelling setup

The model is based on the STORM module [8, 12, 19, 20] using BOUT++ [21, 22]. In this section, we first discuss the simplified 3D straight field line SOL geometry and then we present the drift ordered fluid equations.

The direction along the magnetic field is denoted by z. The target is at $z = \pm L_z = \pm L_\parallel$, where sheath boundary conditions are enforced. Due to the symmetry of the system, only half of the domain is simulated, namely $z = [0, L_z]$. At $z = 0$, symmetry boundary conditions are applied. As the filament is seeded symmetrically, using the symmetry condition is sufficient, which has been verified.

In addition to the parallel direction, the domain is spanned by the radial direction denoted by x and the bi-normal direction, denoted by y. The length along the magnetic field is $L_z = 10$ m, and is resolved by $n_z = 64$ grid points. In the perpendicular direction, the length is $L_x = L_y = 10\delta_\perp$, i.e. dependent on the perpendicular extent of the filament $\delta_\perp$. The resolution is $n_x = n_y = 128$. For $\delta_\perp = 20$ mm, this gives a grid spacing of $dx = 1.562\,5$ mm. The filament size of $\delta_\perp = 20$ mm was chosen as it is both close to the critical size δ^* (introduced later), but also similar to the size experimentally observed in MAST [12, 19].

The STORM model is a drift ordered full fluid model, following the approach of Simakov and Catto [23, 24]. The equations are given in Bohm units [12]. The time is normalized using the ion gyro frequency Ω_i, lengths with the gyro radius $\rho_\mathrm{s} = c_\mathrm{s}/\Omega_\mathrm{i}$ and speeds with the speed of sound $c_\mathrm{s} = \sqrt{T_\mathrm{e}/m_\mathrm{e}}$.

The model consists of the electron density n continuity equation

$$\frac{\partial n}{\partial t} = \frac{\nabla\phi \times \vec{b}}{B} \cdot \nabla n - \nabla_\parallel(Vn) + \mu_n \nabla^2 n - gn\frac{\partial \phi}{\partial y} + g\frac{\partial nT}{\partial y} + \Gamma^\mathrm{ion} - \Gamma^\mathrm{rec} \tag{1}$$

with the potential ϕ being the Laplacian inversion $\omega = \nabla_\perp^2 \phi$ of the vorticity. B is the magnitude of the magnetic field, and $\vec{b}$ is its direction. μ_n is the diffusion coefficient for the electron density. The terms with g are terms due to curvature, which are artificially reintroduced, to drive the filaments. g is a constant related to the radius of curvature R_c as $g = \frac{2}{R_\mathrm{c}} \approx 1.33\ \mathrm{m}^{-1}$. Γ^ion, Γ^rec and Γ^CX are the ionisation, recombination and charge exchange rates. The equation for the parallel electron velocity V is

$$\frac{\partial V}{\partial t} = \frac{\nabla\phi \times \vec{b}}{B} \cdot \nabla V - V\nabla_\parallel V + \mu\nabla_\parallel\phi - \frac{\mu}{n}\nabla_\parallel nT + n\mu\eta_\parallel(U - V) - 0.71\mu\nabla_\parallel T - \frac{V}{n}\Gamma^\mathrm{ion} \tag{2}$$

where the ion–electron mass ratio is $\mu = m_\mathrm{i}/m_\mathrm{e}$. The parallel ion–electron resistivity is given by $\eta_\parallel$. The equation for the parallel ion velocity U is:

$$\frac{\partial U}{\partial t} = \frac{\nabla\phi \times \vec{b}}{B} \cdot \nabla U - U\nabla_\parallel U - \nabla_\parallel\phi - \eta_\parallel n(U - V) + 0.71\nabla_\parallel T - \frac{U}{n}\Gamma^\mathrm{ion} - \frac{U}{n}\Gamma^\mathrm{CX} \tag{3}$$

and the equation for the electron temperature T is

$$\frac{\partial T}{\partial t} = \frac{\nabla\phi \times \vec{b}}{B} \cdot \nabla T - V\nabla_\parallel T + \frac{2}{3}\left(\frac{-1}{n}\nabla_\parallel q_\parallel + 0.71(U - V)\nabla_\parallel T - T\nabla_\parallel V + \frac{\kappa_\perp}{n}\nabla_\perp^2 T + \eta_\parallel n(U - V)^2 - \frac{2}{3}gT\frac{\partial\phi}{\partial y} - \frac{2}{3}g\frac{T^2}{n}\frac{\partial n}{\partial y}\right) - \frac{7}{3}gT\frac{\partial T}{\partial y} - \frac{2}{3}gV^2\frac{1}{\mu n}\frac{\partial nT}{\partial y} - \frac{T}{n}\Gamma^\mathrm{ion}. \tag{4}$$

The parallel heat conduction is given by $q_\parallel$ and $\kappa_\perp$ is the perpendicular heat transport coefficient. The equation for the

vorticity ω is

$$\frac{\partial \omega}{\partial t} = \frac{\nabla\phi \times \vec{b}}{B} \cdot \nabla\omega - U\nabla_{\parallel}\omega + \nabla_{\parallel}(U - V) + \frac{U - V}{n}\nabla_{\parallel} n + \mu_{\omega}\nabla^2\omega + \nabla_{\perp}\mu_{\omega} \cdot \nabla_{\perp}\omega + \frac{g}{n}\frac{\partial nT}{\partial y} - \nabla_{\perp}^2\phi(\Gamma^{\mathrm{CX}} + \Gamma^{\mathrm{ion}}) - \nabla_{\perp}\phi \cdot \nabla(\Gamma^{\mathrm{CX}} + \Gamma^{\mathrm{ion}}) \tag{5}$$

with the vorticity diffusion coefficient μ_ω given by

$$\mu_{\omega} = (1 + 1.6q^2)\frac{6}{8}\frac{\rho_{\mathrm{i}}^2 n Z^4 \Lambda}{\sqrt{m_{\mathrm{i}}}\epsilon_0^2 3(2\pi T_{\mathrm{i}})^{1.5}} \propto \frac{n}{T^{\frac{1}{2}}} \tag{6}$$

with $\Lambda \approx 13$, Z the ion charge, T_{i} the ion temperature (here $T_{\mathrm{i}} = T$) and the safety factor $q = 7$ [25]. The equation for the neutral density n_{n} is

$$\frac{\partial n_{\mathrm{n}}}{\partial t} = \nabla(D_{\mathrm{n}}\nabla n_{\mathrm{n}}) - \Gamma^{\mathrm{ion}} + \Gamma^{\mathrm{rec}} + S_R - f_l n_{\mathrm{n}}. \tag{7}$$

The diffusion constants, resistivity and neutral rates are calculated self consistently [12]. The diffusion rates, including μ_ω, are calculated from first principles as derived by Fundamenski *et al* [25]; as such, they are expected to be experimentally relevant. The neutral model only includes atomic neutrals. D_2 molecules have been included in previous studies, but that has only been carried out in 2D [26]. In the equation for the neutral density, D_{n} is the neutral diffusion, given by

$$D_{\mathrm{n}}^0 = \frac{v_{\mathrm{th}}^2}{v_{\mathrm{th}}\sigma \mathrm{n}_{\mathrm{n}} + \Gamma^{\mathrm{CX}} + \Gamma^{\mathrm{ion}}} \tag{8}$$

$$D_{\mathrm{n}} = \begin{cases} D_{\mathrm{n}}^0 & \text{if } D_{\mathrm{n}}^0 \geqslant 2D^0 \\ D_{\mathrm{n}}^0/2 + D^0 & \text{if } D_{\mathrm{n}}^0 < 2D^0 \end{cases} \tag{9}$$

with v_{th} deuterium's thermal speed at 300 K and the atomic deuterium–deuterium cross section $\sigma = \pi$ (52.9 pm)^2. The diffusion limiter D^0 is needed to compensate for the lack of pressure in high neutral density regions, in which case an unphysically low diffusion occurs. The term $f_l n_{\mathrm{n}}$ emulates cross field losses. Recycling of the neutrals is proportional to the particle flux at the target $f_T = nU|_{\mathrm{target}}$, the recycling coefficient $f_R = 0.9$ and depends on a Gaussian recycling falloff length $L_R = 1$ m:

$$S_R = \alpha_R f_R f_T \exp(-z^2/L_R^2) \tag{10}$$

where α_R is a normalization constant, ensuring that a fraction f_R of the target flux f_T is recycled along the field line. This non-local model was chosen as the lack of pressure combined with high neutral densities near the target results in low return fluxes of particles back along the field line. This non-local recycling model combined with a limiter for the neutral diffusion D_{n} ensures that the neutral is transported upstream from the target. The recycling model is an extension of the density source previously used in STORM [8, 12, 20].

In the radial direction, Neumann boundary conditions with a zero gradient are enforced, with the exception of ω and ϕ, which are set to the respective background values. The y direction is periodic for all quantities. At the symmetry plane, the velocities U and V are set to zero, whereas for the other quantities, zero gradients are enforced. At the target, magnetic pre-sheath boundary conditions were set. The ions need to reach the speed of sound $U = \sqrt{T}$, and the electrons have to reach at the sheath boundary

$$V = \sqrt{T}\exp(-V_{\mathrm{f}} - \frac{\phi}{T}) \tag{11}$$

where V_{f} is the floating potential [27, 28]. The neutral density is forced to have a vanishing gradient at the target boundary.

3. Background profiles

In order to study the influence of self consistent backgrounds on filaments, a procedure for producing such backgrounds is needed. Filaments will be seeded on these backgrounds, as described in section 4. The backgrounds are an extension of the two-point model. They feature only dependence along the magnetic field, and not in the radial direction. In order to generate the 1D background profiles, the equations presented above were used, with the perpendicular terms dropped and the current forced to be zero. The particle and energy influx was set to an exponential shape to localize the influx at the mid-plane. The magnitude was controlled with a PID controller to achieve a predefined value for upstream temperature and density. A PID controller sets the influx as a function of the instantaneous difference to the predefined value, the integral and the derivative of the difference. It is a commonly used control loop feedback mechanism. For the 3D simulation, the controller is replaced by the steady state value of the background simulation. While setting the value via a Dirichlet boundary condition would be easier in the case of the background profiles, the influx needed for maintaining the background is not known. This causes issues for the filament simulations, as a Dirichlet boundary condition would interact non-trivially with the seeded filament. Further, a Dirichlet boundary condition would concentrate all the influx in a single point instead of spreading it.

In order to generate different profiles, the upstream electron temperature T_0 and upstream electron density n_0 were scanned, which allowed for different SOL regimes to be investigated. Figure 1 shows the temperature and density of the electrons, as well as neutral density. The 12 eV temperature simulations are in the high recycling regime as the temperature drops significantly along the field line. The high temperature simulations are in the low recycling regime (also known as the sheath-limited regime) [29]. Note that these simulations do not feature detachment, which requires a more precise treatment of neutrals.

In order to reduce the interaction of the filaments with neutrals, a second set of background profiles was generated, where the plasma–neutral interaction was limited to ionisation. This allows us to keep the recycling dominated fuelling of the plasma, without the need to change the model, except setting $\Gamma^{\mathrm{CX}} = \Gamma^{\mathrm{rec}} = 0$. Figure 2 shows that in this case, the

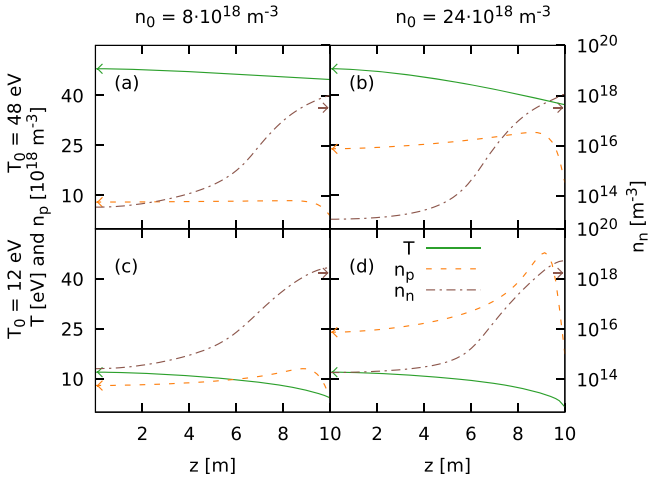

Figure 1. Background plasma profiles, run to steady-state for a set upstream temperature T_0 and density n_0. The sheath is at the right hand side at $L = 10$ m. The mid-plane is at the left side, and is a symmetry plane. The profiles (a) and (b) have an upstream electron temperature of $T_0 = 48$ eV at the mid-plane, while (c) and (d) have an upstream electron temperature of $T_0 = 12$ eV. The upstream background density for (a) and (c) is $n_0 = 8 \times 10^{18}$ m^{-3}, and for (b) and (d) the upstream background density is $n_0 = 24 \times 10^{18}$ m^{-3}. Plasma density n_p (green line) and temperature T (orange dashed) is plotted to the linear scale on the left hand side. The neutral density n_n (brown dash-dotted) is plotted to the log scale on the right hand side.

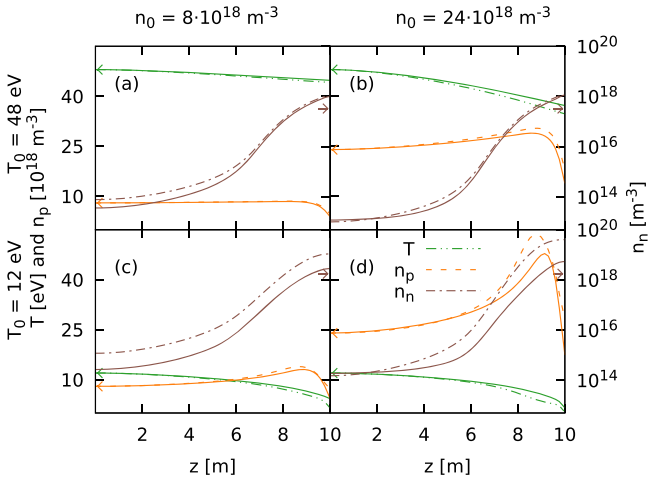

Figure 2. Background plasma profiles—see figure 1 for a detailed description. In addition to the profiles of the full neutral model, shown using continuous lines, the ionisation-only backgrounds are shown using dashed lines.

temperature decreases faster towards the target. This leads to slower ion and electron velocities at the target.

Further, the densities of both the plasma and neutrals is increased. The strongest differences between the models is in the low temperature cases.

4. Filament evolution

The filament is seeded as a density and temperature perturbation on top of the background profiles. The initial shape in the perpendicular direction is Gaussian. The width $\delta_\perp$ is, unless otherwise noted, 20 mm. In the parallel direction, a tanh shape is used with a typical parallel length of 5 m.

Theoretical predictions suggest a scaling of the radial velocity of the filament, that scales with

$$v_\mathrm{r}^s \propto \frac{\delta_\mathrm{p}\sqrt{T_0 + \delta_T}}{n_0 + \delta_n} \tag{12}$$

for the sheath limited regime and

$$v_\mathrm{r}^i \propto \sqrt{\frac{\delta_\mathrm{p}}{n_0 + \delta_n}} \tag{13}$$

for the inertial limited regime [12]. δ_α is the perturbation above the background value α_0, for $\alpha \in n, T$. The pressure perturbation δ_p consists of density and temperature perturbation $\delta_\mathrm{p} = \delta_n T_0 + \delta_T n_0 + \delta_T \delta_n$. To simplify the scalings, we take a density perturbation δ_n equal to the upstream density, n_0, such that $\frac{\delta_n}{n_0} = 1$. Doing the same for the temperature perturbation, setting $\delta_T = T_0$ yields, for the pressure perturbation $\delta_\mathrm{p} = 3 n_0 T_0$. The scalings (12) and (13) reduce to:

$$v_\mathrm{r}^s \overset{\delta_\alpha = \alpha_0}{\propto} \frac{n_0 T_0 \sqrt{T_0}}{n_0} \tag{14}$$

$$v_\mathrm{r}^i \overset{\delta_\alpha = \alpha_0}{\propto} \sqrt{\frac{n_0 T_0}{n_0}} \tag{15}$$

yielding a temperature dependence of $T_0^{\frac{1}{2}}$ for the inertial regime and $T_0^{\frac{3}{2}}$ for the sheath limited regime and no dependence on the density. This convention for the filament perturbations will be adopted throughout this paper. Within the scaling, T_0 describes a 'background' temperature. As the background temperature changes along the magnetic field lines, it is not obvious how this T_0 for the scaling should be calculated.

From the filament simulations, the centre of mass was calculated in the radial direction c_r:

$$c_\mathrm{r} = \frac{\int\int x \Delta n(x, y, z)\, \mathrm{d}x\, \mathrm{d}z}{\int\int \Delta n(x, y, z)\, \mathrm{d}x\, \mathrm{d}z} \tag{16}$$

with

$$\Delta n(x, y, z) = \begin{cases} n(x, y, z) - n_\mathrm{cut}(z) & \text{for } n(x, y, z) - n_\mathrm{cut}(z) > 0 \\ 0 & \text{else} \end{cases} \tag{17}$$

where the cut-off density n_cut was computed by taking the background density of that drift plane. As the initial amplitude near the target is very small, the results shown are measured near the mid-plane. However, the filaments move rigidly, so this velocity is representative of the whole filament.

For each filament simulation, the maximum of the centre-of-mass velocity is computed and compared.

An example of a filament shape is shown in figure 3. The mushrooming behaviour, typical for these filaments [1, 8, 12], can be seen. The filament is not symmetric in the y-direction. This motion in the y-direction, due to the temperature

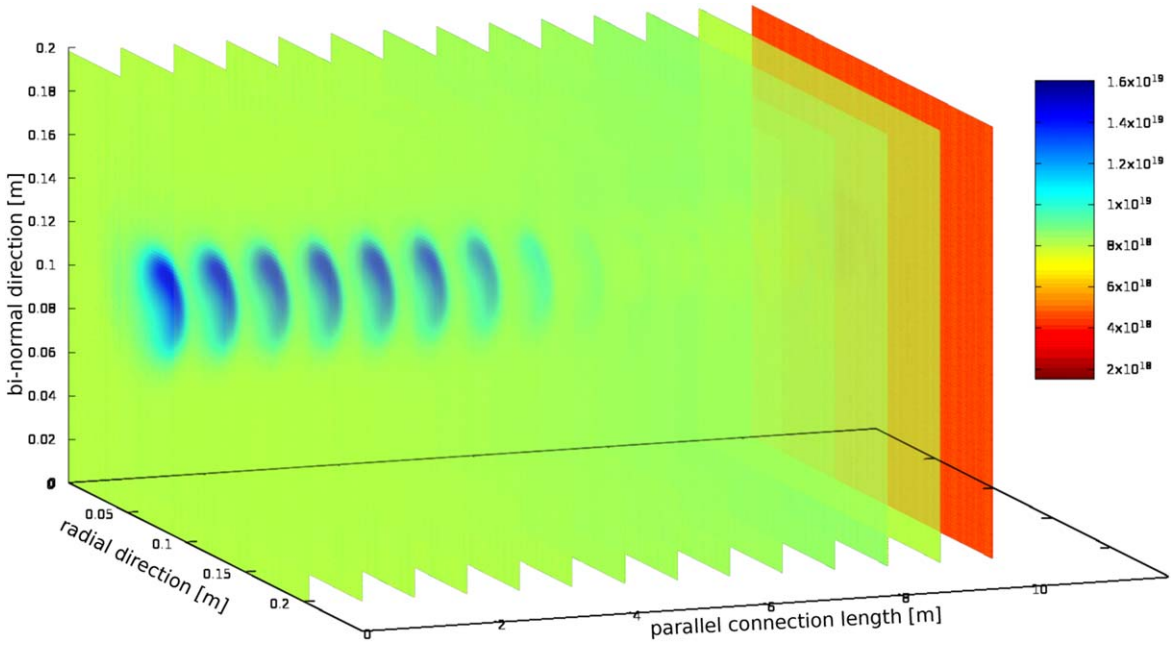

Figure 3. Snapshot of the density ∼7.5 s after the filament was seeded. The upstream background plasma density was $n_0 = 8 \times 10^{18}$ m^{-3} and the upstream electron temperature was $T_0 = 48$ eV. The perpendicular size of the filament was $\delta_\perp = 20$ mm.

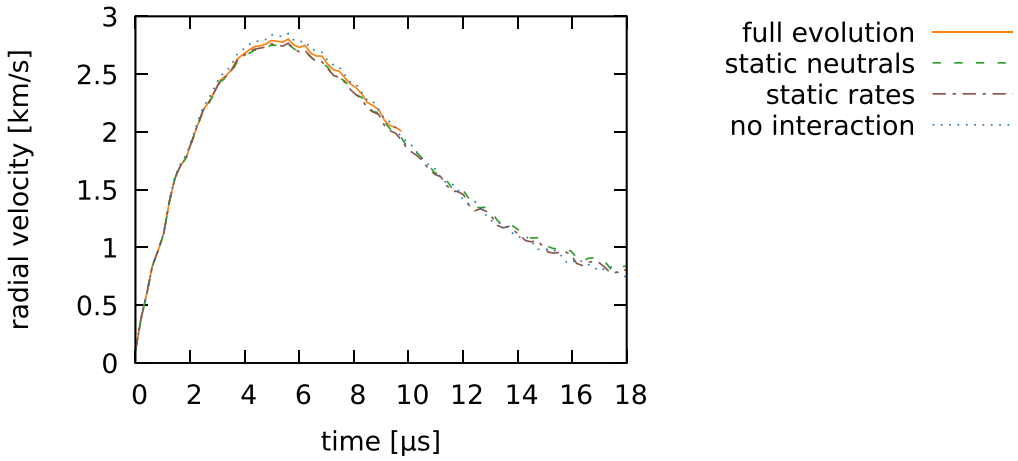

Figure 4. Comparison of different neutral filament interaction models. In the full evolution case (orange line), the neutral density co-evolved with the filament, and the rates were calculated self consistently. In the no interaction case (blue dotted), the neutral term in the vorticity equation was switched off. In the static-rates case (green dashed), the neutral interaction rates Γ^α from the equilibrium profiles were used. In the static neutrals case (brown dash-dotted), the neutrals did not evolve, but the rates were calculated.

perturbation, has been observed and discussed [12, 30]. The temperature perturbation causes an even parity contribution in the potential due to the sheath potential, which causes Boltzmann spinning.

5. Influence on filament velocity

In order to distinguish the direct and the indirect influence of neutrals on filaments, first, different neutral models are compared. This will be followed by a study of the background dependence on filaments, before we conclude with results of the filament size dependence.

5.1. Neutrals

In order to study the direct interaction between the neutrals and the filaments, different neutral–filament interaction models were used.

The results are shown in figure 4. The no interaction case is where the neutral term in the vorticity equation is set to zero. For the other terms, the neutrals are kept static and the neutral rates are calculated self consistently. In the static rates case, the neutral plasma interaction rates, namely charge exchange rate Γ^{CX}, ionisation rate Γ^{ion} and recombination rate Γ^{rec}, are kept at their steady state values. This ensures that areas not affected by the filament are kept at the steady state

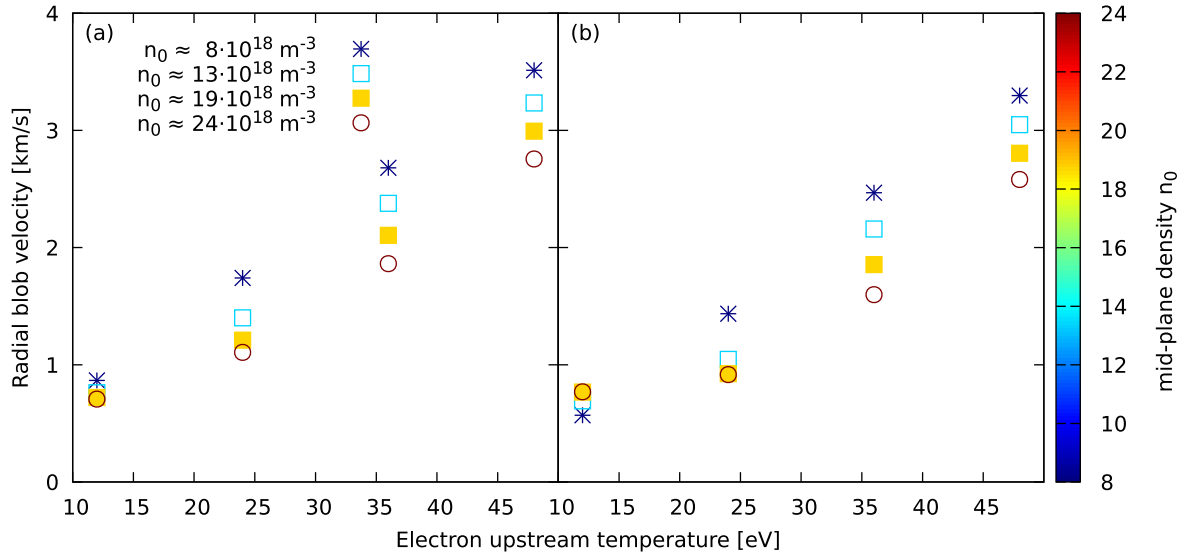

Figure 5. Comparison of the filament velocities for the different set of background profiles, (a) backgrounds with full neutral interaction, and (b) without recombination and charge exchange. The upstream density is colour coded—see legend.

value. The static rates case represents a state where the neutrals are still interacting with the plasma, but the plasma filament interaction is reduced to the neutral plasma background interaction. The interaction is partially further switched on in the case of the static neutrals. There, the neutral profiles did not evolve, but the neutral plasma interaction rates are calculated taking the filament into account. In the full evolution case, the interaction is fully enabled. The neutrals evolve self consistently, and the interaction rates are computed, including both background and filament contributions to density and temperature.

These simulations were done for the different backgrounds shown in figure 1. The result shown in figure 4 is the one with the strongest difference between the velocities, the background profile with high density n_0 and high temperature T_0. The relative reduction for the high density and low temperature case is about half of the velocities shown here. The charge exchange rate is five times as high, as in the high temperature case, while the ionisation rate is about $\frac{1}{4}$. It can be seen that there is only a small difference for the static neutrals and static rates cases. In the case where the neutrals evolve, the filament moves slightly faster. The filament is at its fastest when the neutral drag term in the vorticity equation is switched off. In the case where the neutrals co-evolve with the filament, the filament ionises a part of the neutrals, reducing the neutral density, which explains why the velocity lies between the static case and the no interaction case.

While the impact of neutrals on the filament motion is very small, the impact increased for higher plasma density and plasma temperature. The here observed impact of neutrals is experimentally not measurable, and higher densities are probably needed for the effect to become measurable. The following results are obtained using the static neutral approximation, as this significantly accelerates the computation. With the full neutral model, evolving the filament simulation for $1/\Omega_i$ took ∼3–24 min, while the static neutral model took between 0.3 and 0.6 min per $1/\Omega_i$, resulting in a speed-up between 8 and 40. The deviation from the full neutrals evolution is less than 2% in the conditions featured here, which do not include detachment. As shown by Thrysøe *et al*, D_2 molecules can fuel the atomic neutral density in a filament, which makes the static neutrals approximation even more applicable [26].

In addition to the weak dependence on the direct interaction between filament and neutrals, the filament velocity varies with background conditions. This is shown in figure 5, where on the left filaments were seeded on the backgrounds with full neutral interactions. Also shown is the effect of removing charge exchange and recombination from the simulations. This impacts filament velocity through the change in the backgrounds, indicating that neutrals are important and interact with the filament indirectly via the plasma background. In the next section, the filament velocity's dependence on the background conditions is studied in more detail.

5.2. Background dependence

This section presents the dependence of the filament's radial velocity on the background conditions. Figure 6(a) shows the time evolution of filaments seeded on the background profiles shown in figure 1.

On the right hand side of figure 6 is a plot of the peak of the filament's radial velocity as a function of the upstream temperature. The velocity increases with an increase in temperature. The velocity decreases with increasing density, with the exception of low temperatures where this trend is inverted. As the filaments are seeded such that $\frac{\delta_n}{n}$ stays constant, the density dependence is not expected from the simple scaling analysis shown in section 4.

Earlier studies in STORM looked at the influence of the resistivity [20]. This was done by artificially changing the resistivity. In this study, this is repeated in a self consistent

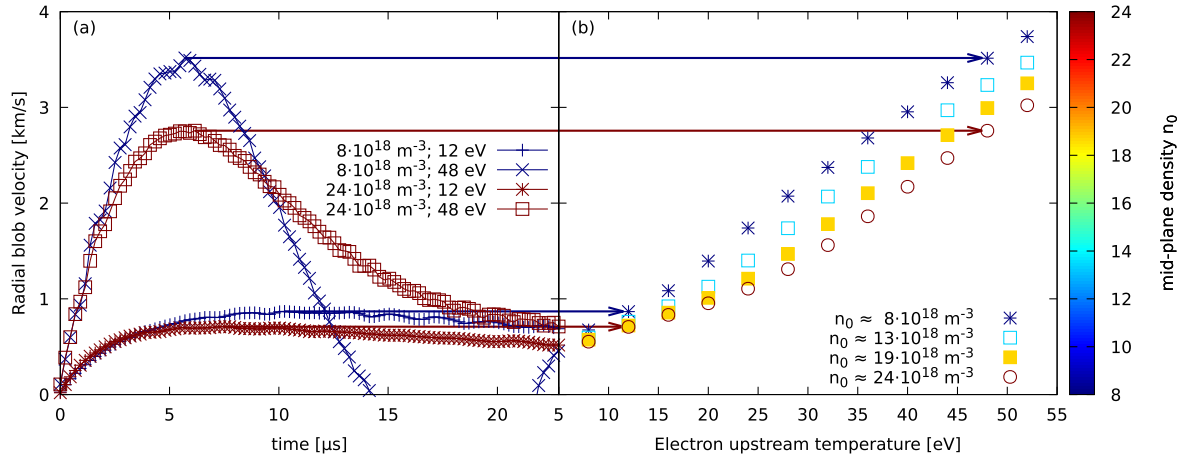

Figure 6. Radial velocity of filaments seeded on different backgrounds. Shown in (a) is the time evolution of the filaments, and (b) shows the peak radial velocities as a function of the upstream temperature. The upstream density is colour coded—see legend.

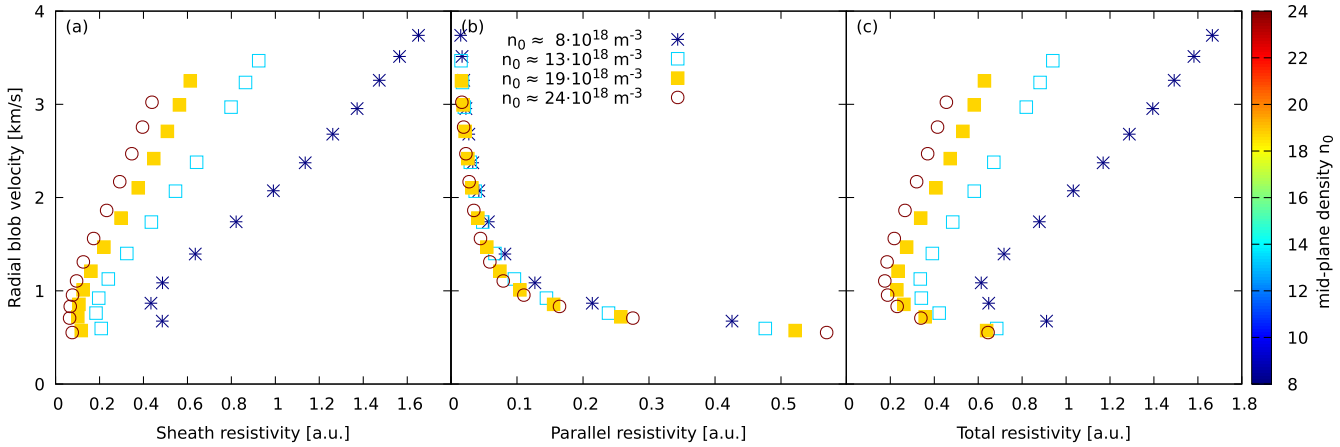

Figure 7. Radial velocity of filaments seeded on different backgrounds. Shown in (a) is the peak velocity as a function of sheath resistivity, (b) as a function of the parallel resistivity, and (c) as a function of total resistivity. The upstream density is colour coded—see legend.

way. In order to change the resistivity, the temperature is changed.

Figure 7 shows the peak velocity as a function of (a) the sheath resistivity, (b) the plasma resistivity integrated along the magnetic field lines, and (c) the total resistivity, consisting of the sum of both. The sheath resistivity is calculated as $\sqrt{T}/n$ following the derivation in [20]. Note that the non-monotonic behaviour below 1 km s^{-1} is because the density at the target reduces quite strongly as the temperature decreases. Therefore the sheath resistivity increases, and the colder temperatures have a higher target resistivity. As the plasma resistivity is a function of the temperature, the scaling in (b) shows a monotonic decreasing behaviour. This is not an effect of the resistivity, since, with an increase in resistivity, the vorticity should increase, which would result in faster filaments [20]. This shows that in this self consistent study, the change in resistivity is less important than the associated change in temperature for the conditions studied here.

The simple scaling analysis shown in section 4 requires a single background temperature; however, the temperature is not constant along the magnetic field lines. Figure 8 shows the filament peak velocities for the different profiles as a function of the upstream temperature, the average temperature and the target temperature. In all cases, a monotonic increase with temperature is observed. In the 'no neutrals' case, the density source has been replaced by an exponentially decaying density source at the target to emulate the ionisation from the neutrals. The systematic, small reduction in filament velocity for the 'no neutrals' case is most likely due to the mismatch in plasma source compared to the full neutral backgrounds. In the case of the target temperature, the different upstream density profiles collapse approximately onto a single line. This suggests that the target temperature is a good scaling quantity for the radial velocity of the filaments studied here. In figure 8(f), the results from the different neutral models are much closer to each other than in figures 8(d)–(e) where they are plotted as a function of the upstream temperature T_0 and the average temperature.

The vorticity equation, which determines the filament radial velocity, represents a balance between parallel, polarization and viscous currents with the driving diamagnetic currents in the filament. Since part of the filament's vorticity is closed via polarization currents, we do not expect such a strong dependence on the target temperature. To study this

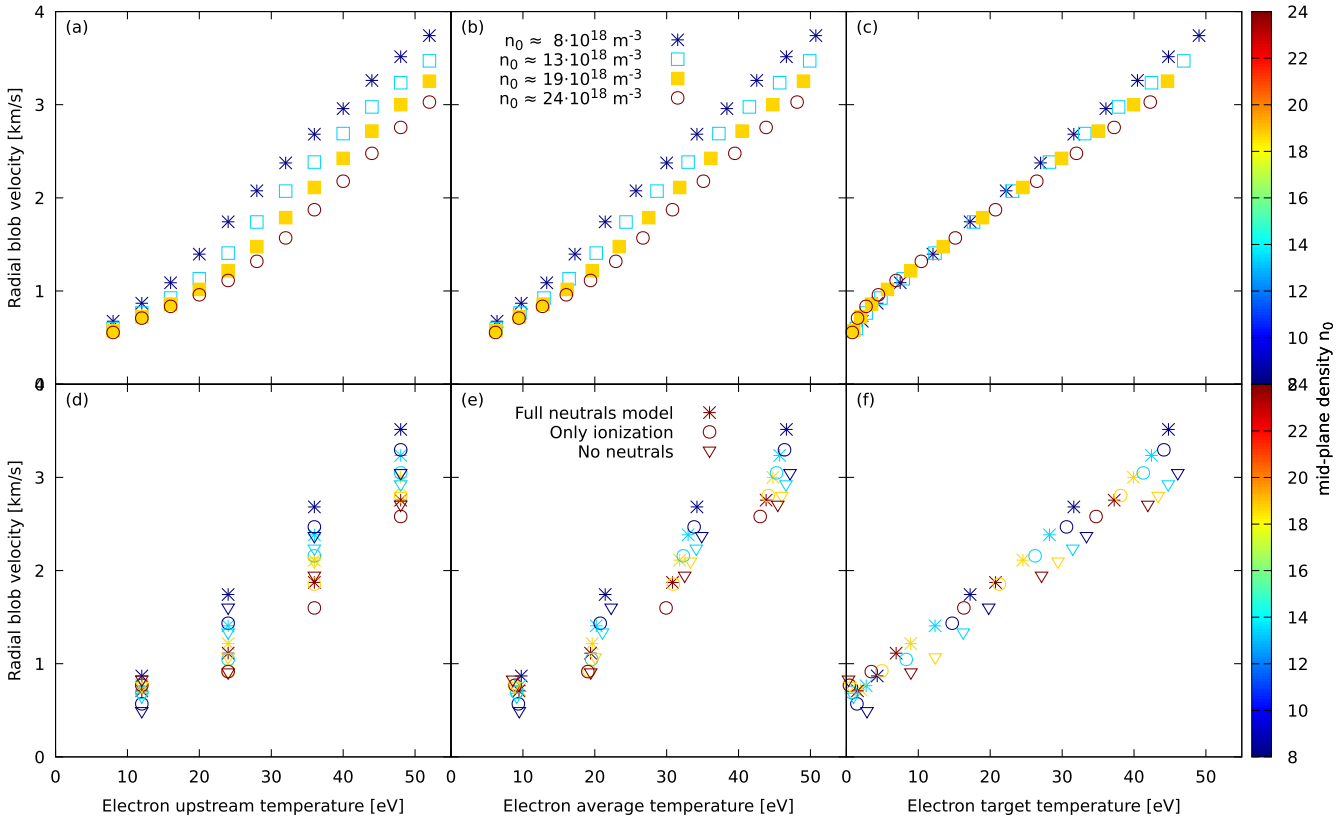

Figure 8. Radial velocity of filaments seeded on different backgrounds. Shown is the peak velocity as a function of temperature. On the top, (a)–(c) are the results with static neutrals, while on the bottom, (d)–(f) are the results for both the full neutral model (stars), the ionisation only model (open circle) and no neutrals model (open triangle). On the left (a), (d), the velocity is plotted against the upstream temperature, in the middle (b), (e), the velocity is plotted against the average temperature and on the right (c), (f), the data is plotted against the target temperature. The upstream density is colour coded, and in (a)–(c) is also shown with different symbols—see legend in (b) or colour-bar.

further, a set of simulations was run, removing the density dependence of the plasma viscosity μ_ω in equation (5). μ_ω has otherwise a linear density dependence, so an increased density leads to an increased diffusion of the vorticity, thereby reducing the drive.

Figure 9 compares the self consistent viscosity simulation (a)–(c) with the ones where the plasma viscosity has no density dependence (d)–(f). The density dependence, when plotted against the upstream temperature, is significantly reduced in figures 9(a), (d). In figure 9(f), the radial velocity is plotted against the target temperature. Although the points do not collapse onto a single line, they are still reasonably close to a single line. This supports the argument that the filaments are not only influenced by the target temperature. It is worth noting that a similar collapse onto one line is apparent in figure 9(d). It seems as if the average temperature strongly influences the filament velocity when the density dependence of the plasma viscosity is removed. In the case of the self consistent viscosity, the target temperature appears to be the dominant influence on the filament velocity. Since the viscosity is acting in the drift plane, it seems unlikely that in one case the target temperature is controlling the filament's dynamics, and in the other, the average temperature is dominant. This supports the argument that the collapse onto a single line is a coincidence, and most likely will not hold true for other conditions. In the simulations presented here, sheath currents play a significant role, therefore the results are not directly applicable to situations where they are suppressed, for example in detached regimes.

Looking at figures 9(a) and (d), removing the density dependence of the plasma viscosity reduces the dependence of the filament velocity on the density. For the remaining density dependence, different reasons come into play. The plasma viscosity still has a temperature dependence and for higher densities, the target temperature drops to lower values than for lower densities, causing a higher viscosity near the target. This shows that the filaments are indeed influenced by the conditions at the target. Note that the filaments have been seeded in a manner such that they are initially unconnected from the sheath. Due to the fast electron motion, they still connect to the target, and are therefore influenced by the plasma conditions at the target.

Another reason for the density dependence is via the neutrals. The study of the direct influence of neutrals suggests that the neutrals have even less of an impact for lower densities. The neutrals can only explain a part of the reduction for the filament's velocity, even for the higher density cases. Further, the background parallel velocity decreases with increasing density. The change in the parallel velocity is stronger for lower temperatures. This can be explained by an increasing importance of recycling in comparison to upstream density fuelling. Although this contribution is only small, it

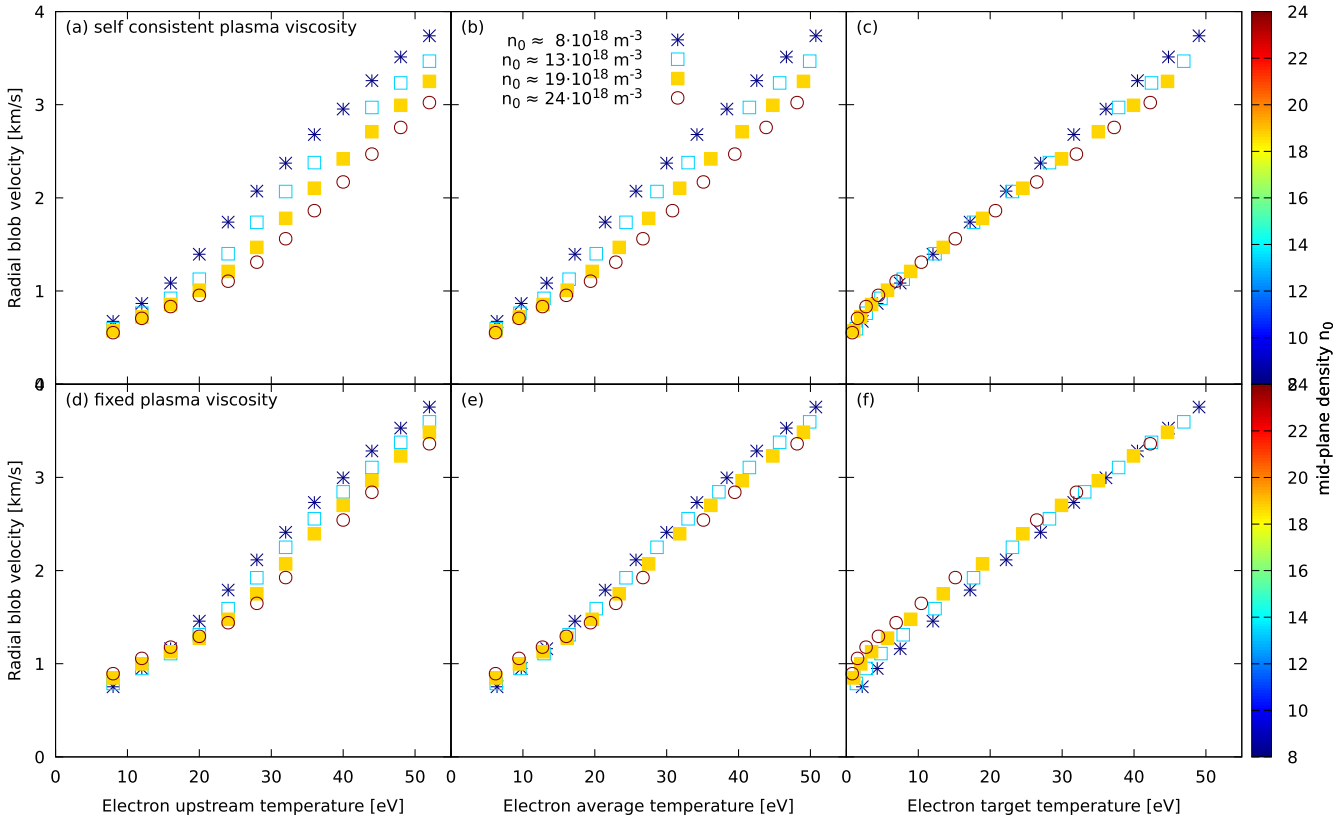

Figure 9. Peak radial velocity of filaments as a function of upstream, average and target temperature. The filaments in (a)–(c) evolved with self consistent plasma viscosity and in (d)–(f) with the density dependence of the plasma viscosity removed. The upstream density is colour coded—see legend in (b) or colour-bar.

might explain, to some extent, the filament velocity crossover at low temperatures, where low densities are slower than high densities. This crossover is observed in the μ_ω case (figure 9(d)) and the ionisation only case (figure 5(b)), while in the full case the density dependence is reduced (figure 9(a)).

Finally, parallel currents play a significant role in the generation of vorticity. The parallel currents are affected by the sheath conditions as they flow through the sheath. Therefore, currents further upstream are also influenced by the sheath temperature. The change in vorticity due to currents is about two to five times as large as the change due to viscosity.

To further test the dependence of the filament velocity on the various temperatures within the system, the upstream and target temperatures have been partially decoupled from one another. This has been achieved by inserting an artificial heat sink localised near the target to control the target electron temperature independent of the upstream temperature.

This was done for the simulations with an upstream temperature of $T_0 = 48$ eV. The temperature close to the target was set to values between 12 eV and 48 eV. The radial velocities are shown in figure 10. Although the filaments were all seeded with the same perturbation of $\delta_T = 48$ eV, the filament velocity agrees with the scaling of the target temperature rather than the upstream temperature. Note that in the cooled target case, the $\nabla n(U - \mathrm{V})$ term is significantly stronger near the target than in the simulations without the target heat sink. Therefore, the vorticity is larger in amplitude near the target than it is further upstream. Furthermore, the viscosity near the target has a strong influence, which appears in the scalings as a strong target temperature dependence. As the target temperature also influences sheath currents, the strong target temperature dependence of the filament velocity is probably due to both the viscosity as well as the sheath currents.

Based on the strong target temperature dependence, it seems tempting to derive a scaling law based on the floating potential, which is dependent on the target temperature. Walkden *et al* shows that the thermal contribution to the filament motion causes filament spinning, rather than advection [12]. The floating potential might be involved in the acceleration of the filament, and might even be responsible for the linear target temperature dependence. But rather than advecting the whole filament, the detailed motion of the filament needs to be considered, thus making this process hard to capture in a scaling law.

5.3. Filament size

To study the influence of the size of the filament on its dynamics, different sized filaments have been seeded, and their motion analysed.

Figure 11(a) presents the scan in filament size. It can be seen that the filament size δ^*, where the filaments are at their fastest for $n_0 = 8 \times 10^{18}$ m^{-3}, is between 14 and 20 mm, and for $n_0 = 24 \times 10^{18}$ m^{-3} is between 20 and 28 mm. The

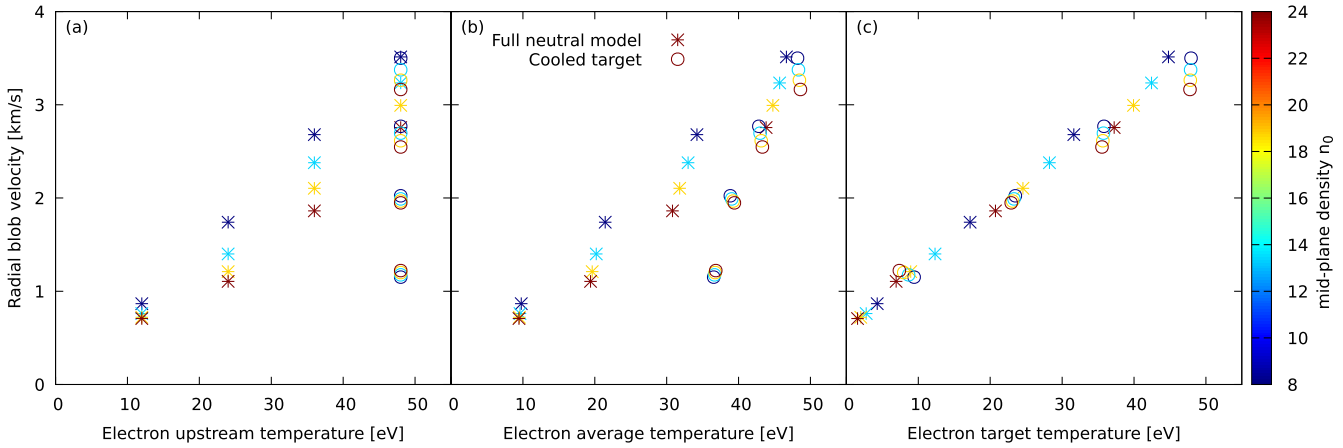

Figure 10. Peak radial velocity of filaments as a function of (a) upstream temperature, (b) average temperature and (c) target temperature. In the simulations plotted with the open circle symbol, the plasma was cooled with an additional heat sink near the target. The upstream density is colour coded—see colour-bar.

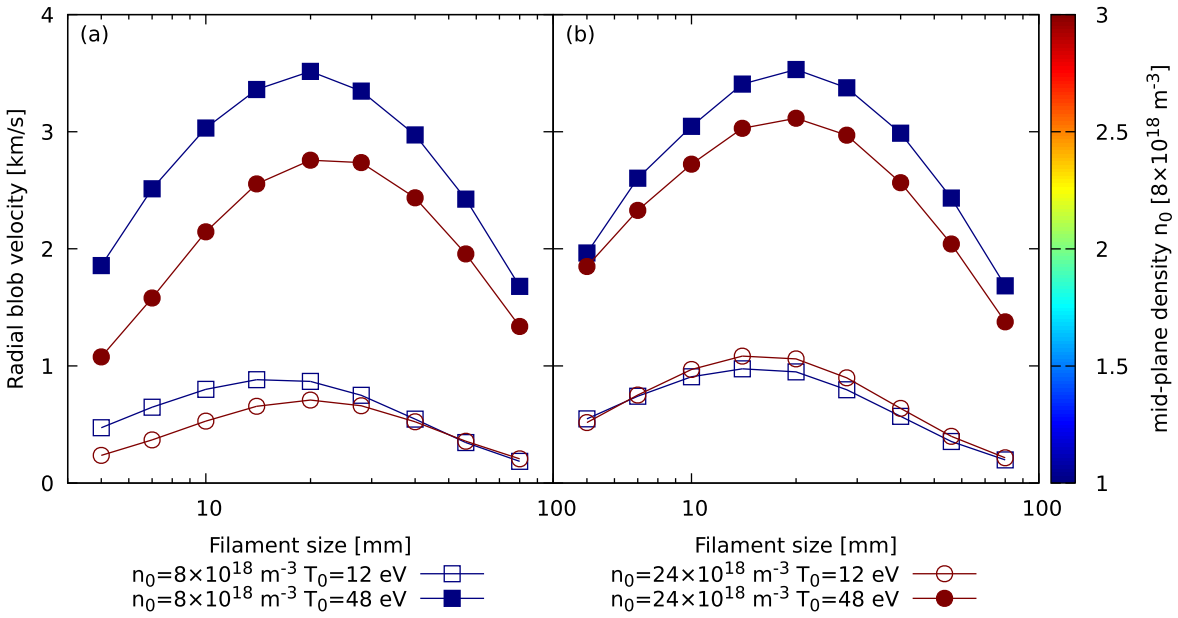

Figure 11. Radial velocity of different sized filaments. Shown is the peak velocity for the four backgrounds from figure 1. The filaments on the left (a) evolved with self consistent plasma viscosity and on the right (b) with the density dependence of the plasma viscosity removed.

position seems to be only influenced by the upstream density n_0, and not by the temperature.

As already done in the previous section, a scan where the plasma viscosity has no density dependence was performed. This is shown in figure 11(b). In this case, the fastest filaments are around $\delta_\perp \approx 20$ mm for the 48 eV cases, and between 14 and 20 mm for the 12 eV case. This shows that the density dependence at this point is due to the density dependence of the plasma viscosity, which has not been included in past studies. Further, a weak temperature dependence of δ^* is observed. From the simple scaling derived in section 4, a temperature dependence but no density dependence is expected, suggesting that future derivations of δ^* should include a self consistent plasma viscosity and currents due to viscosity.

The stronger density dependence of small filaments can be explained by the density dependence of the viscosity. As for small filaments, the currents are closed via currents in the drift plane where viscous currents can contribute. For large filaments, no dependence on the viscosity is observed, as the currents are closed via the sheath.

Figure 12 shows the peak radial velocity for different sized filaments. The ones with size $\delta_\perp \approx \delta^*$ are the fastest ones. The smaller ones and larger ones are significantly slower. The larger ones collapse on a line. This agrees with theory, as the vorticity for larger filaments is mainly closed via sheath currents, therefore a dependence on the sheath conditions is expected. The smaller ones, where the currents are closed mainly via currents in the drift plane, show a stronger dependence on the density. This strong density dependence can be explained by the viscosity. If the density dependence of the viscosity is fixed, they do not collapse that closely onto a single line, suggesting a weaker target dependence compared to larger filaments. As this geometry does not include an X-point, filaments can be connected to the

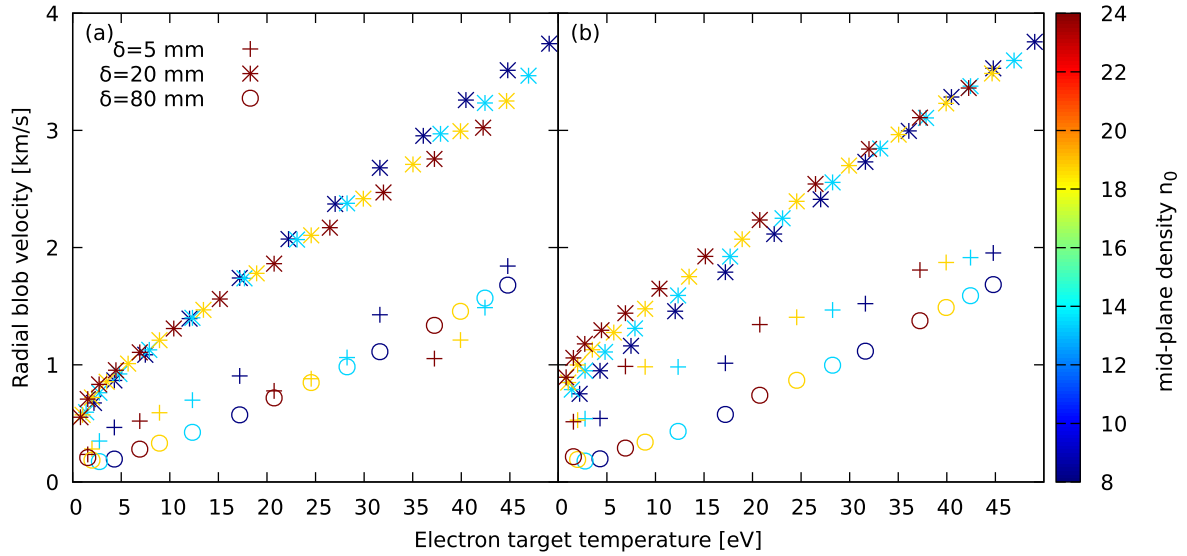

Figure 12. Radial velocity of different sized filaments. Shown is the peak velocity as a function of target temperature for different sized filaments. The $\delta_\perp = 20\,\text{mm} \approx \delta^*$ are similar in size to the ones observed in MAST. Small filaments are denoted by a plus symbol, critical-sized filaments by a star, and large filaments by an open circle. The upstream density is colour coded—see colour-bar. The filaments on the left (a) evolved with self consistent plasma viscosity and on the right (b) with the density dependence of the plasma viscosity removed.

target, and therefore influenced by the target. If a more realistic geometry is used, it is quite likely that, at least for the smaller filaments, the influence of the plasma conditions at the sheath is reduced compared to larger filaments.

6. Summary

Filament radial velocities in the scrape-off layer for different background profiles have been studied. The upstream temperature and density have been varied, resulting in self consistent parallel profiles. The backgrounds do not include gradients in the radial direction. Filaments were seeded on the background profiles, and the radial filament velocity was measured.

It has been shown that the direct interaction between the filament and the neutrals is strongest in the high density and high temperature case, where a weak reduction of velocity was observed, agreeing with the prediction by Theiler *et al* [18]. As the filament motion depends on the background profiles, all filaments were subject to indirect neutral influences via the dependence of the background profiles on neutrals. To accurately capture the filament dynamics, the parallel variation of the background plasma, including interactions with the neutral population, should be included.

Increasing the upstream temperature resulted in a faster radial motion of the filament. The radial velocity also decreased with the increasing upstream density. This can be explained by the reduced target temperature with increasing density, as the target temperature was shown to be the best ordering parameter for the filaments studied here. As the filament perturbation is seeded in a manner such that it is initially unconnected to the sheath, it is the fast electron motion that connects the filament electrically to the sheath. In this way, the target temperature dependence can be explained by the temperature dependence of the plasma viscosity and by sheath currents.

The strong target temperature dependence is not only observed for filament sizes close to the critical size δ^* but also for larger ones. Here, a significant amount of the current is closed via sheath currents. Smaller filaments show a strong dependence on plasma density due to the density dependence of the plasma viscosity. If this influence is reduced, they also show a strong dependence on the sheath temperature. Further, a shift of δ^* with density is observed. This is not expected from scaling laws, but can be explained by the density dependence of the plasma viscosity. This suggests that the plasma viscosity should be included if scalings for δ^* are derived.

The geometry used does not include an X-point or magnetic shear. Furthermore, detachment was not studied here, as a more accurate neutral model would be required. Both these aspects could reduce the target dependence, and further studies are required to validate these findings in the case of detached conditions or in scenarios including high magnetic shear.

Acknowledgments

This work has been carried out within the framework of the EUROfusion Consortium and has received funding from the Euratom research and training programme 2014–2018 under grant agreement No 633053 and from the RCUK Energy Programme (grant number EP/P012450/1). To obtain further information on the data and models underlying this paper, please contact PublicationsManager@ukaea.uk. The views and opinions expressed herein do not necessarily reflect those of the European Commission. Simulations in this paper made use of the ARCHER UK National Supercomputing service (http://archer.ac.uk) under the Plasma HEC Consortium EPSRC grant number EP/L000237/1 and the EUROfusion

High Performance Computer (Marconi-Fusion) through EUROfusion.

ORCID iDs

D Schwörer https://orcid.org/0000-0003-0911-8606
N R Walkden https://orcid.org/0000-0002-0661-5909
H Leggate https://orcid.org/0000-0002-1582-0330
B D Dudson https://orcid.org/0000-0002-0094-4867
F Militello https://orcid.org/0000-0002-8034-4756
T Downes https://orcid.org/0000-0002-7639-5446
M M Turner https://orcid.org/0000-0001-9713-6198

References

[1] D'Ippolito D, Myra J and Zweben S 2011 Convective transport by intermittent blob-filaments: comparison of theory and experiment *Phys. Plasmas* **18** 060501
[2] Roth J *et al* 2009 Recent analysis of key plasma wall interactions issues for ITER *J. Nucl. Mater.* **390–391** 1–9
[3] Boedo J A *et al* 2001 *Phys. Plasmas* **8** 4826–33
[4] Militello F and Omotani J T 2016 On the relation between non-exponential scrape off layer profiles and the dynamics of filaments *Plasma Phys. Control. Fusion* **58** 125004
[5] Yu G Q and Krasheninnikov S I 2003 Dynamics of blobs in scrape-off-layer/shadow regions of tokamaks and linear devices *Phys. Plasmas* **10** 4413–8
[6] Yu G, Krasheninnikov S and Guzdar P 2006 Two-dimensional modelling of blob dynamics in tokamak edge plasmas *Phys. Plasmas* **13** 042508
[7] Garcia O, Bian N and Fundamenski W 2006 Radial interchange motions of plasma filaments *Phys. Plasmas* **13** 082309
[8] Easy L, Militello F, Omotani J, Dudson B, Havlíčková E, Tamain P, Naulin V and Nielsen A H 2014 Three dimensional simulations of plasma filaments in the scrape off layer: a comparison with models of reduced dimensionality *Phys. Plasmas* **21** 122515
[9] Jovanović D, Shukla P and Pegoraro F 2008 Effects of the parallel electron dynamics and finite ion temperature on the plasma blob propagation in the scrape-off layer *Phys. Plasmas* **15** 112305
[10] Halpern F D, Cardellini A, Ricci P, Jolliet S, Loizu J and Mosetto A 2014 Three-dimensional simulations of blob dynamics in a simple magnetized torus *Phys. Plasmas* **21** 022305
[11] Angus J R, Umansky M V and Krasheninnikov S I 2012 Effect of drift waves on plasma blob dynamics *Phys. Rev. Lett.* **108** 215002
[12] Walkden N R, Easy L, Militello F and Omotani J T 2016 Dynamics of 3D isolated thermal filaments *Plasma Phys. Control. Fusion* **58** 115010
[13] Bisai N and Kaw P K 2013 Role of ion temperature on scrape-off layer plasma turbulence *Phys. Plasmas* **20** 042509
[14] Leddy J, Willett H V and Dudson B D 2016 Simulation of the interaction between plasma turbulence and neutrals in linear devices *Nucl. Mater. Energy* **12** 994–8
[15] Bisai N and Kaw P 2016 Role of neutral gas in scrape-off layer of tokamak plasma in the presence of finite electron temperature and its gradient *Phys. Plasmas* **23** 092509
[16] Wersal C and Ricci P 2015 A first-principles self-consistent model of plasma turbulence and kinetic neutral dynamics in the tokamak scrape-off layer *Nucl. Fusion* **55** 123014
[17] Thrysøe A S, Tophøj L E H, Naulin V, Rasmussen J J, Madsen J and Nielsen A H 2016 The influence of blobs on neutral particles in the scrape-off layer *Plasma Phys. Control. Fusion* **58** 044010
[18] Theiler C, Furno I, Ricci P, Fasoli A, Labit B, Müller S H and Plyushchev G 2009 Cross-field motion of plasma blobs in an open magnetic field line configuration *Phys. Rev. Lett.* **103** 065001
[19] Schwörer D, Walkden N, Leggate H, Dudson B, Militello F, Downes T and Turner M 2017 Influence of plasma background including neutrals on scrape-off layer filaments using 3D simulations *Nucl. Mater. Energy* **12** 825–30
[20] Easy L, Militello F, Omotani J, Walkden N and Dudson B 2016 Investigation of the effect of resistivity on scrape off layer filaments using three-dimensional simulations *Phys. Plasmas* **23** 012512
[21] Dudson B, Umansky M, Xu X, Snyder P and Wilson H 2009 BOUT++: a framework for parallel plasma fluid simulations *Comput. Phys. Commun.* **180** 1467–80
[22] Dudson B D *et al* 2015 BOUT++: recent and current developments *J. Plasma Phys.* **81** 1
[23] Simakov A N and Catto P J 2003 Drift-ordered fluid equations for field-aligned modes in low-β collisional plasma with equilibrium pressure pedestals *Phys. Plasmas* **10** 4744–57
[24] Simakov A N and Catto P J 2004 Erratum: 'drift-ordered fluid equations for field-aligned modes in low-β collisional plasma with equilibrium pressure pedestals' (2003 *Phys. Plasmas* 10 4744) *Phys. Plasmas* **11** 2326–2326
[25] Fundamenski W, Garcia O, Naulin V, Pitts R, Nielsen A, Rasmussen J J, Horacek J, Graves J and (JET EFDA contributors) 2007 Dissipative processes in interchange driven scrape-off layer turbulence *Nucl. Fusion* **47** 417
[26] Thrysøe A, Madsen J, Naulin V and Rasmussen J J 2018 Influence of molecular dissociation on blob-induced atom density perturbations *Nucl. Fusion* **58** 096005
[27] Chodura R 1982 Plasma-wall transition in an oblique magnetic field *Phys. Fluids* **25** 1628
[28] Stangeby P C 1995 The bohm-chodura plasma sheath criterion *Phys. Plasmas* **2** 702–6
[29] Stangeby P C *et al* 2000 *The Plasma Boundary of Magnetic Fusion Devices* vol 224 (Bristol: Institute of Physics Publishing)
[30] Myra J, D'ippolito D, Krasheninnikov S and Yu G 2004 Convective transport in the scrape-off-layer by nonthermalized spinning blobs *Phys. Plasmas* **11** 4267–74